THE JOURNAL OF BIOLOGICAL CHEMISTRY
Vol. 278, No. 26, Issue of June 27, pp. 24125–24131, 2003

Printed in U.S.A.

Importance of the Conserved Aromatic Residues in the Scorpion α-Like Toxin BmK M1

THE HYDROPHOBIC SURFACE REGION REVISITED*

Received for publication, November 22, 2002, and in revised form, April 4, 2003
Published, JBC Papers in Press, April 13, 2003, DOI 10.1074/jbc.M211931200

Yan-Mei Sun‡§, Frank Bosmans§¶, Rong-Huan Zhu‡, Cyril Goudet¶, Yu-Mei Xiong‡, Jan Tytgat¶, and Da-Cheng Wang‡‖

From the ‡Center for Molecular Biology, Institute of Biophysics, Chinese Academy of Sciences, 15 Datun Road, Beijing 100101, People's Republic of China and the ¶Laboratory of Toxicology, University of Leuven, E. Van Evenstraat 4, B-3000 Leuven, Belgium

About one-third of the amino acid residues conserved in all scorpion long chain Na^+ channel toxins are aromatic residues, some of which constitute the so-called "conserved hydrophobic surface." At present, in-depth structure-function studies of these aromatic residues using site-directed mutagenesis are still rare. In this study, an effective yeast expression system was used to study the role of seven conserved aromatic residues (Tyr^5, Tyr^{14}, Tyr^{21}, Tyr^{35}, Trp^{38}, Tyr^{42}, and Trp^{47}) from the scorpion toxin BmK M1. Using site-directed mutagenesis, all of these aromatic residues were individually substituted with Gly in association with a more conservative substitution of Phe for Tyr^5, Tyr^{14}, Tyr^{35}, or Trp^{47}. The mutants, which were expressed in *Saccharomyces cerevisiae* S-78 cells, were then subjected to a bioassay in mice, electrophysiological characterization on cloned Na^+ channels ($Na_v1.5$), and CD analysis. Our results show an eye-catching correlation between the LD_{50} values in mice and the EC_{50} values on $Na_v1.5$ channels in oocytes, indicating large mutant-dependent differences that emphasize important specific roles for the conserved aromatic residues in BmK M1. The aromatic side chains of the Tyr^5, Tyr^{35}, and Trp^{47} cluster protruding from the three-stranded β-sheet seem to be essential for the structure and function of the toxin. Trp^{38} and Tyr^{42} (located in the β_2-sheet and in the loop between the β_2- and β_3-sheets, respectively) are most likely involved in the pharmacological function of the toxin.

Scorpion neurotoxins targeting voltage-gated sodium channels are single chain polypeptides composed of 60–70 amino acids cross-linked by four disulfide bridges. They have been divided into two major classes, α- and β-toxins. Scorpion α-toxins, the most extensively studied group, can prolong the action potential by slowing the inactivation of Na^+ currents with no direct effect on activation (1–3).

According to their different pharmacological properties, the α-toxins can be further divided into three subgroups, classical α-, α-like, and insect α-toxins (4, 5). The classical α-toxins (*e.g.* AaH II and Lqh II) are highly toxic to mammals, whereas the insect α-toxins (*e.g.* Lqh α insect toxin) are highly toxic to insects. The more recently characterized α-like toxins (*e.g.* Lqh III and BmK M1) act on both mammals and insects, but are unique in their inability to bind to rat synaptosomes despite a high toxicity by intravenous injection. Although three-dimensional structures for the classical α-toxins (6, 7), α-like toxins (8, 9), and insect α-toxins (10) have been elucidated, in-depth structure-function studies of these long chain toxins using site-directed mutagenesis are still rare, mainly because of folding problems; and the focus has often been on the charged residues in the toxins (11, 12). Here, we report the importance of the conserved aromatic residues in α-toxins identified by mutagenesis analysis using the α-like toxin BmK M1 as template.

BmK M1 is a toxin from the venom of the scorpion *Buthus martensii* Karsch, which resides in eastern Asia, and is composed of 64 amino acids cross-linked by four disulfide bridges (3, 7). BmK M1 has been the subject of different studies: its three-dimensional structure was determined by x-ray crystallography at 1.7-Å resolution (8); the pharmacological properties of Na^+ channels have recently been investigated (13); and gene cloning and expression of wild-type BmK M1 have also been carried out (14, 15).

Alignment of the amino acid sequences of several α-toxins shows that seven aromatic residues, including Tyr^5, Tyr^{14}, Tyr^{21}, Tyr^{35}, Tyr^{42}, Trp^{38}/Tyr^{38}, and Trp^{47}/Tyr^{47}, are notably conserved (Fig. 1*A*) (5). In a previously performed structural analysis, a conserved hydrophobic surface (CHS)[1] was identified (7). The CHS is assumed to be part of the functional site of scorpion toxins targeting sodium channels (16, 17). Tyr^5, Tyr^{35}, and Trp^{47} are located on the so-called Face A surface of the toxin (CHS). Tyr^{14} and Tyr^{21} are situated on the surface opposite to Face A, called Face B. Trp^{38} and Tyr^{42} are located in the β_2-sheet and in the loop between the β_2- and β_3-sheets, respectively (Fig. 1*B*).

Seven of the 15 residues conserved in scorpion toxins (5) are aromatic residues and have been studied in this work. Based on an efficient yeast expression system (15), the importance of the above-mentioned aromatic residues in the scorpion toxin BmK M1 was analyzed by site-directed mutagenesis. The results from mutagenesis and expression, characterization, bioassays, and electrophysiological analysis of the mutants are reported here. Based on these findings, the important role of these conserved aromatic residues is discussed.

* This work was supported by State Basic Research Program Grant G19990756, the National Natural Science Foundation of China, Fonds voor Wettenschappelijk Onderroek Grant G.0081.02, Flanders/People's Republic of China Bilateral Grant BIL00/06, and a Katholieke Universiteit Leuven post-doctoral fellowship (to C. G.). The costs of publication of this article were defrayed in part by the payment of page charges. This article must therefore be hereby marked "*advertisement*" in accordance with 18 U.S.C. Section 1734 solely to indicate this fact.

§ Both authors contributed equally to this work.
‖ To whom correspondence should be addressed. Tel.: 86-10-6488-8547; Fax: 86-10-6488-8560; E-mail: dcwang@sun5.ibp.ac.cn.

[1] The abbreviations used are: CHS, conserved hydrophobic surface; rBmK, recombinant BmK; Tricine, *N*-[2-hydroxy-1,1-bis(hydroxymethyl)ethyl]glycine; AaH, *Androctonus australis Hector*; Lqh, *Leiurus quinquestriatus hebraeus*.

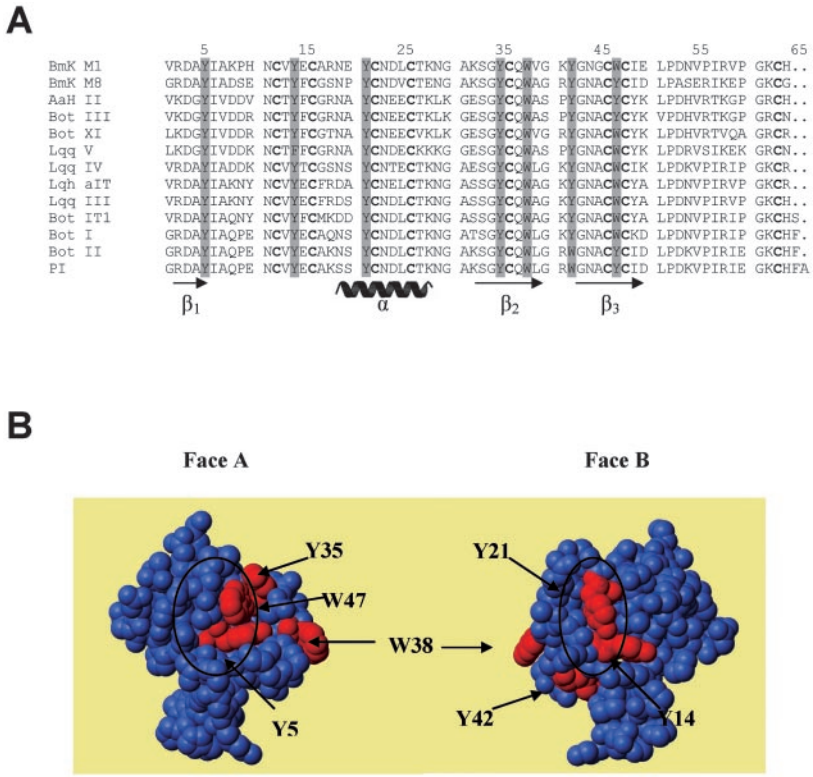

FIG. 1. *A*, amino acid sequences of representative scorpion α-toxins. The sequences are aligned at their cysteine residues. The conservative aromatic residues are highlighted in *gray*. *Bot*, *Buthus occitanus tunetanus*; *Lqq*, *Leiurus quinquestriatus quinquestriatus*; *PI*, *Pandinus imperator*. *B*, the conserved aromatic residues substituted with Gly or Phe. Face A, which corresponds to the CHS, is indicated by the *ellipse* in the *left model*. The substituted amino acids of Face B are indicated by the ellipse in the *right model*. The orientations of Faces A and B are related to each other by a 180° rotation around the vertical axis of the molecule. The figures were produced using MOLMOL 2K.1 (27).

EXPERIMENTAL PROCEDURES

Strains, Materials, and Animals—Plasmid pVT102U/α, *Escherichia coli* strain TG1, and *Saccharomyces cerevisiae* strain S-78 (Leu2, Ura3, Rep4) were used. Restriction endonucleases and T4 DNA ligase were obtained from Roche Applied Science (Mannheim Germany). Primers were synthesized by Sangon (Shanghai, China). *Taq* DNA polymerase and Klenow fragment were obtained from MBI. CM32-cellulose cation-exchange and Sephasil® peptide C_{18} reversed-phase (12-μm ST4.6/250) columns were from Whatman and Amersham Biosciences AB (Uppsala, Sweden), respectively. All other chemicals were at least analytical grade and were purchased from Merck or Sigma. The mice used for the bioassay were ICR mice from the Beijing Center for Experimental Animals.

Site-directed Mutagenesis of BmK M1—The cDNA of BmK M1 was previously cloned (14) and inserted into pVT102U/α (15). According to the sequence of pVT102U/α-BmK M1, two primers were designed: primer 1 (5′-CGTCTAGATAAAAGAAATTCTGTTCGG-3′, including a KEX2 protease linker and an *Xba*I restriction site) and primer 2 (5′-CGAAGCTTTTAATGGCATTTTCCTGGTAC-3′, with a *Hin*dIII site). The substitute residue for all aromatic residues was glycine. In addition, the more conservative substitutions of phenylalanine for Tyr^5, Tyr^{14}, Tyr^{35}, and Trp^{47} were carried out.

The mutagenic primers used to generate the desired mutations were as follows: Y5G, 5′-CGTCTAGATAAAAGAAATTCTGTTCGGGATGCT-***GGT***ATTGCCAAGCCCCATAACTGT; Y5F, 5′-CGTCTAGATAAAAGA-AATTCTGTTCGGGATGCT***TTC***ATTGCCAAGCCCCATAACTGT; Y14G, 5′-AACTGTGTA***GGT***GAATGTGCT (positive strand) and 5′-AG-CACATTC***ACC***TACACAGTT (negative strand); Y14F, 5′-AACTGTGT-A***TTC***GAATGTGCT (positive strand) and 5′-AGCACATTC***GAA***TACA-CAGTT (negative strand); Y21G, 5′-AGAAATGAA***GGT***TGCAACGAT-TTATGT (positive strand) and 5′-ACATAAATCGTTGCA***ACC***TTCAT-TTCT (negative strand); Y35G, 5′-AAGAGTGGC***GGT***TGCCAATGG (positive strand) and 5′-CCATTGGCA***ACC***GCCACTCTT (negative strand); Y35F, 5′-AAGAGTGGC***TTC***TGCCAATGG (positive strand) and 5′-CCATTGGCA***GAA***GCCACTCTT (negative strand); W38G, 5′-T-ATTGCCAA***GGT***GTAGGTAAA (positive strand) and 5′-TTTACCTAC-***ACC***TTGGCAATA (negative strand); Y42G, 5′-GTAGGTAAA***GGT***GG-AAATGGC (positive strand) and 5′-GCCATTTCC***ACC***TTTACCTAC (negative strand); W47G, 5′-AATGGCTGC***GGT***TGCATAGAG (positive strand) and 5′-CTCTATGCA***ACC***GCAGCCATT (negative strand); and W47F, 5′-AATGGCTGC***TTC***TGCATAGAG (positive strand) and 5′-CTCTATGCA***GAA***GCAGCCATT (negative strand).

Using pVT102U/α-BmK M1 (recombinant BmK (rBmK) M1) as template along with primer 2 and the mutagenic primer, mutants Y5G and Y5F were created by one-step PCR. Other mutants (Y14G, Y14F, Y21G, Y35G, Y35F, W38G, Y42G, W47G, and W47F) were obtained by three-step PCR. A pair of mutagenic primers was applied in the first or second PCR with primer 1 or 2, respectively, to create two intermediate products, which shared an identical sequence. After treatment with Klenow fragment, two intermediate products acted as primers for each other, and extension of this overlap by DNA polymerase created the full-length mutant, which had the mutation at the desired position. All PCR products were purified by gel excision.

Expression and Purification of Mutants—After digestion with *Xba*I and *Hin*dIII, the mutated cDNA gene was inserted into plasmid pVT102U/α and transformed into *E. coli* TG1 competent cells. The recombinant plasmid pVT102U/α-mutant was extracted, sequenced, and transformed into *S. cerevisiae* S-78 using the LiCl method (18). The expression of the mutants was carried out using a described previously procedure (15). After fermentation, the supernatant of the culture was adjusted to pH 4.2 with acetic acid. The sample was directly applied to a CM32-cellulose cation-exchange column (2.8 × 14 cm), which was equilibrated with 0.1 M sodium acetate at a flow rate of 1 ml/min. Upon reaching a steady base line, the column was washed by stepwise elution with 0.2, 0.3, and 0.5 N NaCl equilibration buffer. The 0.5 N NaCl fraction was directly applied to a Sephasil® peptide C_{18} reversed-phase column. Buffer A contained 0.1% trifluoroacetic acid in water; buffer B contained 0.1% trifluoroacetic acid in acetonitrile. The C_{18} column was eluted with a linear gradient of 0–80% buffer B for 15 column volumes. Reversed-phase chromatography was carried out using an ÄKTA purifier chromatography system (Amersham Biosciences AB).

Molecular Mass Determination—The molecular masses of the purified mutants were obtained using a Finnigan LCQ ion-trap mass spectrometer (ThermoQuest, San Jose, CA) equipped with an electrospray ionization source. The spray voltage was 4.50 kV. Calculations were performed using the program provided by the manufacturer.

Bioassay—Using 0.9% NaCl as a negative control and rBmK M1 as a positive control, the toxicity of the mutants was determined in mice (male, specified pathogen free level, 18–20 g of body weight). Each group consisted of 10 mice. Various doses of toxin mutants were dissolved in 0.9% NaCl and injected into the mice through the tail vein. Survival times (times between injection and death), reaction, and doses were recorded. Evaluation of toxicity was based on the determination of LD_{50} (the dose capable of statistically killing 50% of the mice) according to the method of Meier and Theakston (19).

Expression in Xenopus Oocytes, Electrophysiological Recordings, and Analysis—The human $Na_v1.5$ gene was subcloned into pSP64T (20). For

TABLE I
Overview of the results for the 11 BmK M1 mutants

Toxin	Expression	Toxicity (LD_{50})	Relative toxicity	EC_{50}
	mg/liter	*mg/kg*	*%*	*μM*
Wild-type rBmK M1	~3	0.53	100	0.50
Y5G	Trace			
W47G	None			
Y21G	1-2	1.01	52	1.0
Y35G	1-2	16.04	3	5.0
W38G	1-2	>25	<2	>100
Y42G	1-2	>25	<2	>100
Y14G	1-2	>25	<2	>100
Y14F	≈3	0.75	71	3.4
Y35F	≈3	0.97	55	0.7
W47F	9-10	2.34	23	3.1
Y5F	≈3	13.44	4	>100

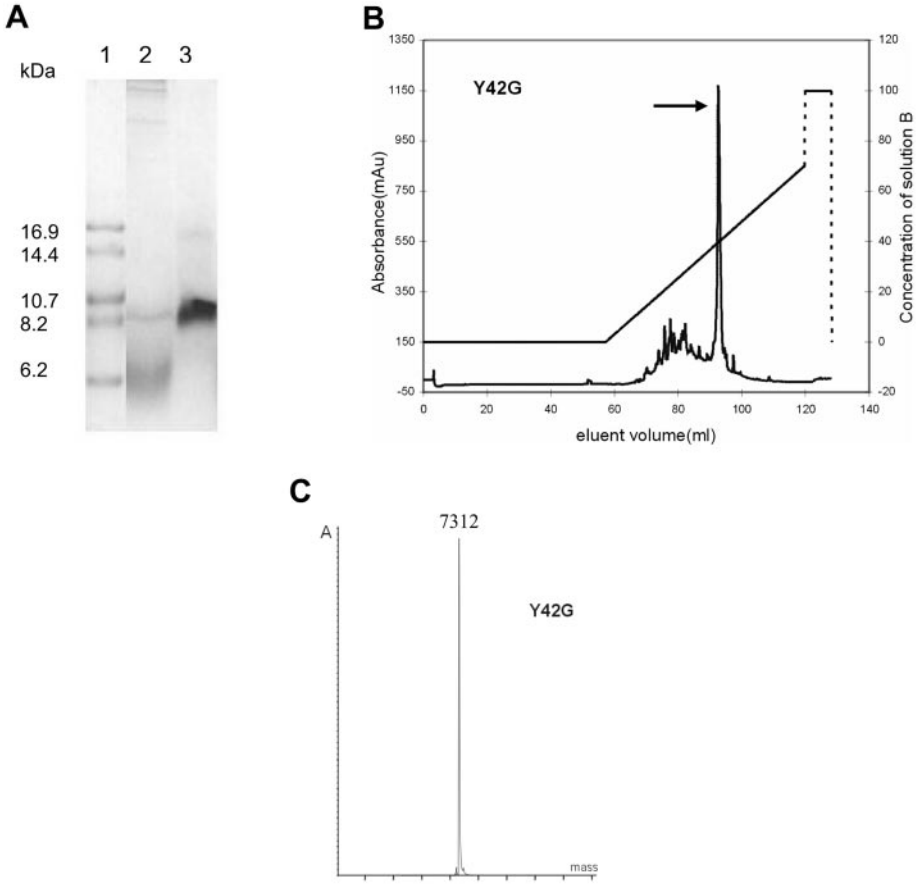

FIG. 2. **As an example, the entire purification process of Y42G is shown.** *A*, Tricine/SDS-PAGE before and after purification. The protein bands were stained with Coomassie Brilliant Blue R-250. *Lane 1*, molecular mass markers; *lane 2*, fermentation supernatant of Y42G, *lane 3*, purified Y42G. *B*, purification of Y42G by reversed-phase chromatography. *C*, Finnigan LCQ ion-trap mass spectra of Y42G. The mass spectra of the other mutants are not shown. *mAU*, milliabsorbance units.

in vitro transcription, pSP64T/$Na_v1.5$ was first linearized by *Xba*I. Using the large-scale SP6 mMESSAGE mMACHINE transcription kit (Ambion Inc.), capped cRNAs were synthesized from the linearized plasmids. The *in vitro* synthesis of cRNA encoding histone H1 and the isolation of *Xenopus* oocytes were done as described previously (21). Oocytes were injected with 50 nl of $Na_v1.5$ cRNA solution at a concentration of 1 ng/nl using a Drummond microinjector.

Whole cell currents from oocytes were recorded using the two-microelectrode voltage clamp technique between 1 and 3 days after injection. Voltage and current electrodes were filled with 3 M KCl. Resistances of both electrodes were kept as low as possible (~0.1–0.2 megaohms). Experiments were performed using a GeneClamp 500 amplifier (Axon Instruments, Inc.) controlled by a pClamp data acquisition system (Axon Instruments, Inc.). Currents were sampled at 10 kHz and filtered at 5 kHz using a four-pole low-pass Bessel filter. Digital leak subtraction of the current records was carried out using a P/2 protocol. The bath solution composition was 96 mmol/liter NaCl, 2 mmol/liter KCl, 1.8 mmol/liter $CaCl_2$, 2 mmol/liter $MgCl_2$, and 5 mmol/liter HEPES (pH 7.4). This solution was supplemented with 50 mg/liter gentamycin sulfate for incubation of the oocytes. All experiments were performed at room temperature (20–22 °C).

Circular Dichroism Measurements—Samples used for analyses were dissolved in 20 mM phosphate buffer (pH 7) at a concentration of 1.0 mg/ml. Circular dichroism spectra were recorded on a Jasco J-720 spectropolarimeter. Spectra were run at 25 °C from 250 to 200 nm using a quartz cell 0.5 mm in length. Data were collected at 0.5-nm intervals with a scan rate of 50 nm/min. All CD spectra resulted from averaging four scans. The final spectrum was corrected by subtracting the corresponding base-line spectrum obtained under identical conditions. Spectra were smoothed by the instrument's software. The secondary structure content was estimated by standard Jasco CD analysis.

RESULTS

Mutation, Expression, and Purification—Single point mutants Y14G, Y14F, Y21G, Y35G, Y35F, W38G, Y42G, W47G,

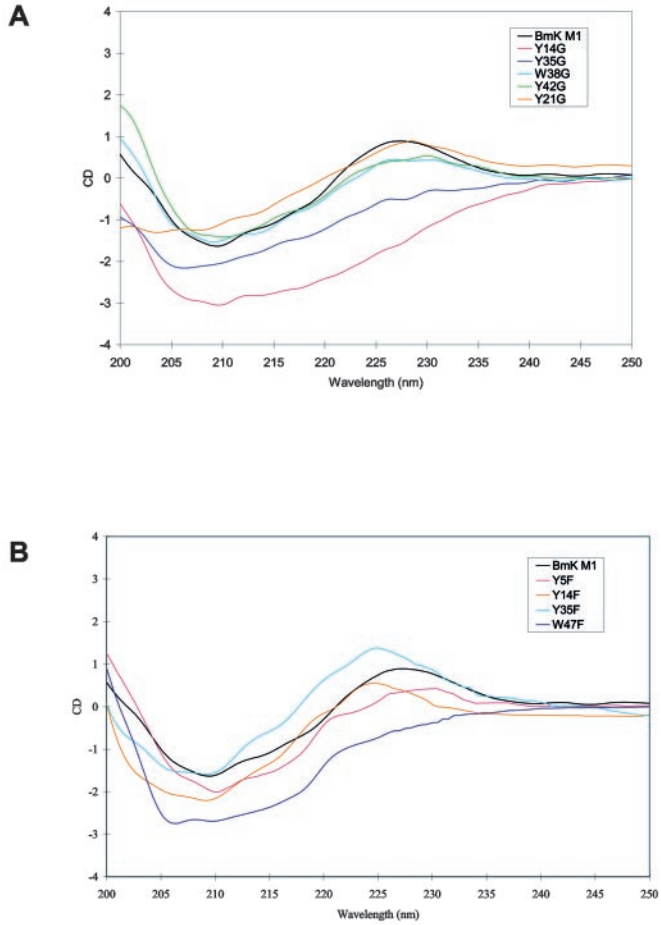

FIG. 3. **CD spectra of BmK M1 and its mutants.** *A*, spectra of BmK M1, Y14G, Y21G, Y35G, W38G, and Y42G; *B*, spectra of BmK M1, Y5F, Y14F, Y35F, and W47F. Measurement was carried out in the UV range of 250–200 nm on a Jasco J-720 system at pH 7.0 with a concentration of 1.0 mg/ml at room temperature.

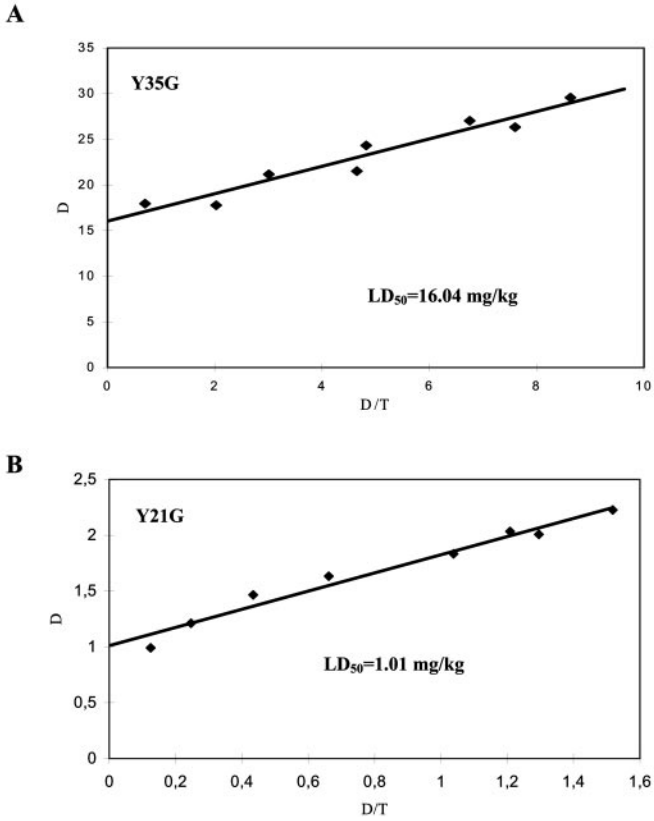

FIG. 4. **As an example, the LD50 values for mutants Y35G (*A*) and Y21G (*B*) are given.** *D*, dose (milligrams/kg) of recombinant toxin used in the experiments; *T*, survival time (minutes) of mice after injection of toxin. The LD_{50} values were determined using the method of Meier and Theakston (19). The point where the regression intersects the *ordinate* is the LD_{50}. The determined LD_{50} values shown for the expressed mutants Y35G and Y21G were 16.04 and 1.01 mg/kg, respectively.

and W47F were created by three-step PCR. Mutants Y5G and Y5F were produced by one-step PCR. The target gene was expressed using the pVT102U/α vector. Tricine/SDS-PAGE analyses of yeast cultures demonstrated that mutants Y5G, Y5F, Y14G, Y14F, Y21G, Y35G, Y35F, W38G, Y42G, and W47F were expressed and secreted into the medium. Mutant Y5G could not be used in the following characterization because its expression level was in a trace amount. Mutant W47G could not be expressed at all. The expression levels of the five glycine mutants Y14G, Y21G, Y35G, W38G, and Y42G were ~1–2 mg/liter of culture medium. For three of the mutants with the conservative phenylalanine substitution (Y5F, Y14F, and Y35F), the expression levels were ~3 mg/liter, comparable to that of unmodified rBmK M1 (~3 mg/liter). Remarkably, the amount of W47F in the culture medium was 9–10 mg/liter, which is about three times the value of rBmK M1 (Table I). Apparently, the conservative phenylalanine mutations of Tyr^5 and Trp^{47} changed the expression levels of mutants Y5G and W47G from a trace or nothing at all to the normal level or to even a high level.

Expressed mutants were purified by a simple and efficient protocol. One liter of culture (10 g/liter yeast extract, 20 g/liter bacteriological peptone, 20 g/liter glucose, pH after sterilization of 6.5) was harvested and initially purified by chromatography on a CM32 cation-exchange column. The next step of purification was carried out on a C_{18} column. The elution peaks corresponding to target mutants were pooled and lyophilized. The Tricine/SDS-polyacrylamide gels and the mass spectra showed a high purity of the final products. As an example, the entire purification process of Y42G is shown at the following stages: Tricine/SDS-PAGE before and after purification (Fig. 2*A*), reversed-phase chromatography (Fig. 2*B*), mass spectrometry (Fig. 2*C*).

Molecular Mass—The molecular masses of the purified variants were measured with the Finnigan LCQ ion-trap mass spectrometer. The individual peaks showed that the molecular masses of mutants Y5F, Y14G, Y14F, Y21G, Y35G, Y35F, W38G, Y42G, and W47F were 7403, 7312, 7403, 7315, 7312, 7403, 7289, 7312, and 7380 Da, respectively (Y42G is shown as an example in Fig. 2*C*). This corresponded well with the estimated molecular masses of the mutants: 7404, 7313, 7404, 7313, 7313, 7404, 7290, 7313, and 7380 Da, respectively.

Conformational Analysis—The CD spectra of rBmK M1 and its mutants in the UV range of 250–200 nm are shown in Fig. 3. Compared with native BmK M1, the CD spectra of Y14G and Y35G dramatically changed (Fig. 3*A*), indicating that there are apparent changes in the secondary structures of these two mutants. The secondary structure estimation (J-700 for Windows Secondary Structure Estimation, Version 1.10.00) indicates that mutation Y14G interrupts both the α-helix and β-sheet, whereas mutation Y35G interrupts only the β-sheet. In both cases, the estimated random coils show a significant increase.

For Y21G, W38G, and Y42G, the CD spectra show that the secondary structures have almost not changed compared with the native toxin (Fig. 3*A*). It seems that the loss of the aromatic side chains in these mutants does not alter the general struc-

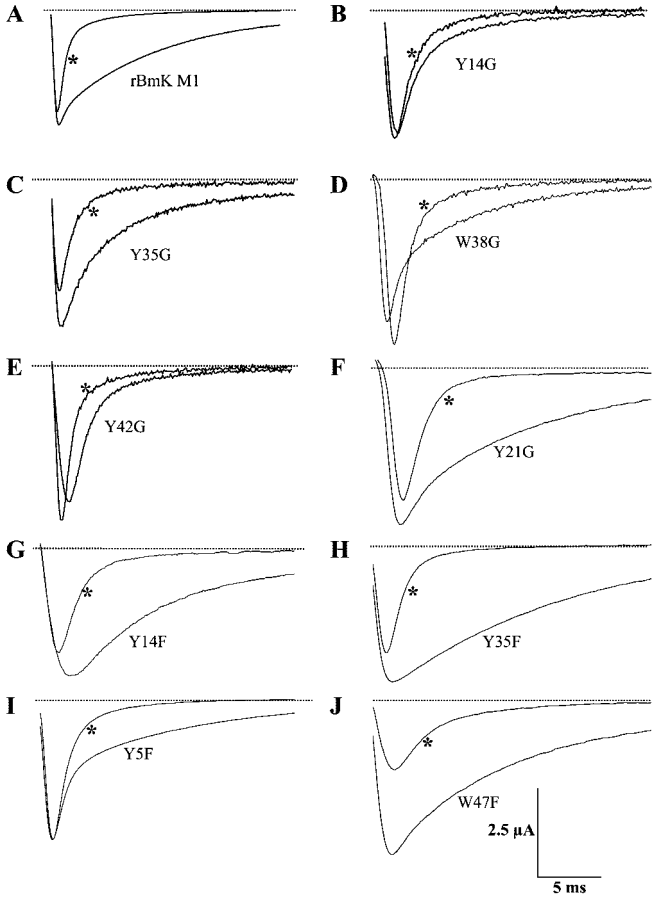

FIG. 5. **Effect of rBmK M1 and its aromatic amino acid mutants on the inactivation kinetics of $Na_v1.5$ channels expressed in *Xenopus* oocytes.** Current traces were evoked by a depolarization step to −20 mV over 25 ms from a holding potential of −90 mV in the absence (*) and presence of the following toxins: 5 μM rBmK M1 (*A*), 30 μM Y14G (*B*), 30 μM Y35G (*C*), 30 μM W38G (*D*), 50 μM Y42G (*E*), 5 μM Y21G (*F*), 10 μM Y14F (*G*), 7.5 μM Y35F (*H*), 100 μM Y5F (*I*), and 10 μM W47F (*J*).

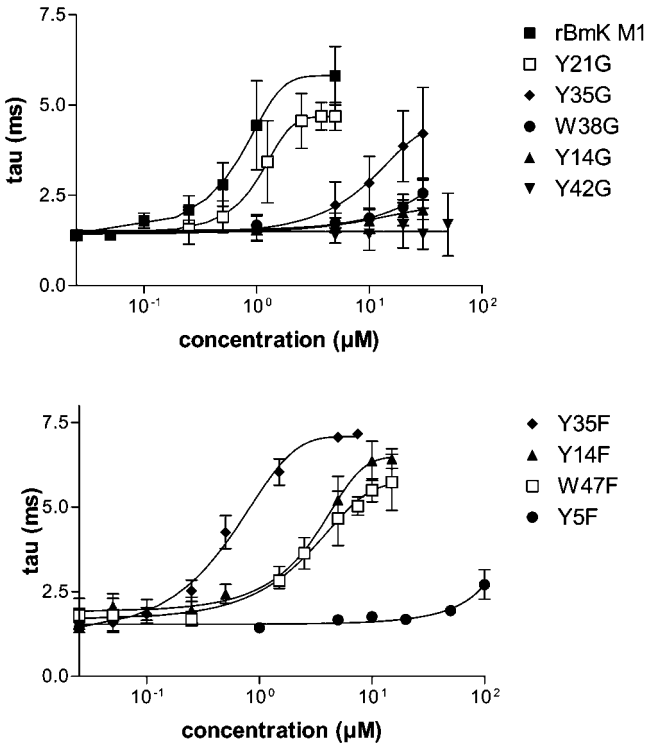

FIG. 6. **Concentration dependence of the effect of rBmK M1 and its mutants on $Na_v1.5$ channels.** The averaged time constant of inactivation (τ) is plotted *versus* the concentration of rBmK M1 and its mutants. For rBmK M1, Y21G, and Y35G, the EC_{50} values determined by a sigmoidal fit were 0.50 ± 0.03, 1.02 ± 0.15, and 5.05 ± 0.36 μM, respectively (*upper panel*). The EC_{50} values for Y14G, W38G, and Y42G could not be determined. For Y14F, Y35F, and W47F, the EC_{50} values were 3.36 ± 0.48, 0.71 ± 0.09, and 3.1 ± 0.3 μM, respectively (*lower panel*). The EC_{50} value for Y5F could not be determined. Time constants of inactivation were calculated from a single exponential fit from peak current to end of trace (25 ms) of a current trace clamped at −20 mV. Data represent the mean ± S.E. of at least three experiments for each concentration.

ture of the toxin. Regarding mutants with the conservative phenylalanine substitution, the CD spectra show small alterations for Y5F, Y14F, and Y35F, but large changes for W47F compared with wild-type BmK M1 (Fig. 3*B*).

Bioassay—The mice showed typical symptoms of envenomation after injection with rBmK M1. The LD_{50} determined by the method of Meier and Theakston (19) was ~0.53 mg/kg, which is consistent with that of native BmK M1 (16). Excluding W47G and Y5G, which were not expressed and expressed only in trace amounts, respectively, the other nine mutants (Y5F, Y14G, Y14F, Y21G, Y35G, Y35F, W38G, Y42G, and W47F) were used for bioassays. Each purified mutant was injected into the mice through the tail vein at different doses to determine the LD_{50} value (Fig. 4 and Table I).

Mutants Y14G, W38G, and Y42G showed no detectable toxicity even at a dose of 25 mg/kg, which is 47 times the LD_{50} of rBmK M1 (Table I). Mutant Y35G lost most of its toxicity (LD_{50} = 16.04 mg/kg, which is 30 times the LD_{50} of rBmK M1). In contrast, the LD_{50} of Y21G was only twice that of rBmK M1 (Fig. 4 and Table I).

For the phenylalanine mutants, the toxicities of Y14F (71%) and Y35F (55%) were in the same order as that of unmodified rBmK M1. The toxicity of W47F displayed a certain decrease (23%). The toxicity of Y5F was dramatically reduced to 4% in comparison with unmodified rBmK M1 (Fig. 4 and Table I).

Effect of rBmK M1 and Its Aromatic Amino Acid Mutants on Voltage-gated Na^+ Channels—Fig. 5 displays the effects of rBmK M1 and mutants Y14G, Y35G, W38G, Y42G, Y21G, Y14F, Y35F, Y5F, and W47F on $Na_v1.5$ Na^+ channels expressed in *Xenopus laevis* oocytes. The currents displayed were evoked by a depolarization step to −20 mV from a holding potential of −90 mV. The current traces recorded after the addition of the toxin reveal that rBmK M1 induced a slowing of the inactivation process of Na^+ currents. This effect appeared a few seconds after the addition of the toxin and continued until reaching a steady state after 4–5 min. Under control conditions, the inactivation kinetics of $Na_v1.5$ currents were rapid, and almost no remaining currents were visible at the end of the traces, after 25 ms. The toxin-induced slowing of inactivation was evaluated by a single exponential fit (pClamp Version 8) of the current decay after the peak. The time window for each fit was manually set from the peak current to the end of the trace (25 ms). Under steady-state conditions, the time constant of inactivation (τ) calculated by a single exponential fit increased from 1.4 ± 0.2 ms (n = 33) under control conditions to 4.4 ± 1.2 ms (n = 6) after the addition of 1 μM rBmK M1 and to 5.8 ± 0.8 ms (n = 3) after the addition of 5 μM rBmK M1. This represents an increase of ~414% in the time constant τ in the presence of 5 μM rBmK M1. As shown in Fig. 5, all of the glycine mutants except Y21G were less efficient even at high concentrations (30 and 50 μM) in slowing the inactivation kinetics of $Na_v1.5$ channels compared with the wild-type toxin. Mutants Y14G and Y42G of rBmK M1 were the least effective in slowing the

inactivation of the channel. The time constants of inactivation were 2.1 ± 0.3 ms (n = 3) and 1.7 ± 0.3 ms (n = 4) after the addition of 30 μM Y14G and 50 μM Y42G, respectively, corresponding to 150 and 121% of the time constants under control conditions, respectively. The addition of 30 μM W38G increased the time constant of inactivation to 2.6 ± 0.4 ms (n = 3), corresponding to 186% of the control value. Y35G was the second most effective mutant, increasing the τ value to 4.2 ± 1.3 ms (n = 3) at a concentration of 30 μM, corresponding to 300% of the control value. Y21G was the most effective mutant, increasing the τ value to 4.7 ± 0.4 ms (n = 3) at a concentration of 5 μM, corresponding to 335% of the control value.

As shown in Fig. 5, all of the phenylalanine mutants except Y5F had about the same efficacy in $Na_v1.5$ as rBmK M1. The time constants of inactivation were 5.4 ± 0.6 ms (n = 4), 7.1 ± 0.4 ms (n = 4), and 5.8 ± 0.6 ms (n = 3) after the addition of 10 μM W47F, 7.5 μM Y35F, and 10 μM Y14F, respectively, corresponding to 385, 507, and 414% of the time constants under control conditions, respectively. Y5F was the least effective in slowing the inactivation of the Na^+ channel. The time constant of inactivation was only 2.3 ± 0.6 ms (n = 3) after the addition of 100 μM, corresponding to 165% of the control value. The effects of rBmK M1 and some of its mutants on the peak Na^+ current and time to peak were somewhat variable (oocyte-dependent) and not further analyzed.

The slowing of inactivation induced by rBmK M1 and its mutants was concentration-dependent (Fig. 6). The EC_{50} values of rBmK M1, Y21G, Y35G, Y35F, Y14F, and W47F were determined by a sigmoidal fit of the τ-V relationship as displayed in Fig. 6. The EC_{50} values determined for rBmK M1, Y21G, Y35G, Y35F, Y14F, and W47F were 0.50 ± 0.03, 1.02 ± 0.15, 5.05 ± 0.36, 0.71 ± 0.09, 3.36 ± 0.48, and 3.1 ± 0.3 μM, respectively. The EC_{50} value determined in this study for rBmK M1 is slightly higher than the EC_{50} value determined for the native BmK M1 toxin (0.2 μM) in one of our previous studies (13). Y21G was comparable to native rBmK M1. Y35G was ~30% less efficient in slowing the inactivation kinetics of $Na_v1.5$ channels compared with wild-type rBmK M1. The EC_{50} value of Y35G was at least 10 times higher than that of rBmK M1. The EC_{50} values of the phenylalanine mutants were comparable to that of rBmK M1, except Y5F. As shown in Fig. 6, the EC_{50} values of Y14G, Y42G, W38G, and Y5F could not be determined because the highest concentrations used did not reach a maximal effect in the dose-response curve.

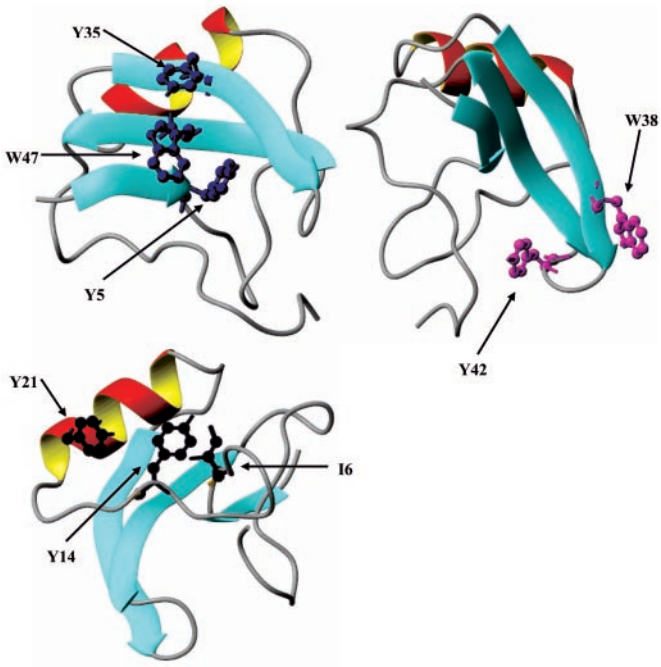

FIG. 7. **Possible role of the conserved aromatic residues identified by site-directed mutagenesis analysis.** Tyr^{35} and Trp^{47} (structural importance) and Tyr^5 (functional and structural importance), belonging to the CHS (Face A), are indicated in the *upper left model*. Residues putatively involved in the functionality (Trp^{38} and Tyr^{42}) are shown in the *upper right model*. Tyr^{14} (functional and structural importance) and Tyr^{21}, belonging to Face B, are shown in the *lower left model*. Ile^6 is also indicated in *blue* to show the interaction with Tyr^{14}. The figures were produced using MOLMOL 2K.1 (27).

DISCUSSION

When the three-dimensional structures of the scorpion toxins CsE V3 and AaH II were elucidated ~20 years ago, the CHS, mainly including Tyr^5, Tyr^{35}, and Trp^{47}/Tyr^{47}, was proposed to be responsible for the pharmacological effect of these toxins (17, 22, 23). Although the CHS is found in all scorpion toxin structures known today, this assumption required experimental identification. The individual residues in this cluster (*e.g.* Trp^{45} in AaH II and Tyr^{49} in Lqh α insect toxin) have been assessed by chemical modification (24) and mutagenesis analysis (11, 25) and shown to play an important role in bioactivity. In this study, seven aromatic residues, including three amino acids of this cluster, were analyzed by site-directed mutagenesis. Correlating the high impact substitution of glycine to the more conservative mutation of phenylalanine, our results clearly indicate that these conserved aromatic residues are specifically involved in either or both pharmacological function and structural stability.

Aromatic Residues Possibly Involved in Pharmacological Function—The bioassay showed that the toxicity of W38G and Y42G was dramatically reduced (Table I). In concordance, electrophysiological analysis showed that W38G and Y42G were the least effective in slowing the inactivation of the sodium channel. The EC_{50} could not be determined because the highest concentration available could not induce a maximal effect in the dose-response curves (Figs. 5 and 6). Simultaneously, the CD spectra of these two mutants show the least alteration in comparison with that of unmodified BmK M1 (Fig. 3*A*). These results can be used to speculate that the conserved aromatic residues Trp^{38} and Tyr^{42} are involved in the functional performance of the toxin.

Tyr^{42} is located in the loop between the β_2- and β_3-sheets (Fig. 7). Considering that this loop is remarkably different in sequence and structure between α- and β-toxins (7, 17), this aromatic residue may be related to the preference for the distinct target site of α-toxins.

Aromatic Residues Possibly Involved in Structural Stability—The non-expression of W47G and the extremely unstable expression of Y5G indicate that these two residues are essential for the general structure of the toxin. The polypeptide chain of the toxin cannot be folded correctly without these aromatic side chains. Y35G could be expressed in an amount comparable to the wild type, but its toxicity was reduced dramatically (Table I). In agreement with the obtained LD_{50} value in mice, the corresponding EC_{50} value of Y35G in $Na_v1.5$ was 10 times higher than that of rBmK M1. The CD spectrum also changed dramatically (Fig. 3*A*), indicating an alteration of the secondary structure of Y35G. Interestingly, the conservative phenylalanine substitution mutants were expressed very well. Y5F and Y35F were present in the culture medium in an amount of ~3 mg/liter, comparable to rBmK M1. The expression level of W47F was high (9–10 mg/liter) in comparison with rBmK M1 (Table I). Compared with rBmK M1, alterations in the CD spectra were milder for Y5F and Y35F, but severe for W47F (Fig. 3*B*). In addition, the bioassay, in concordance with

the electrophysiological characterization, showed that the bioactivities of all of the phenylalanine mutants (although in different degrees) were significantly higher than those of the mutants that lost their aromatic side chains by substitution with glycine (Table I). Hence, by constructing and thoroughly comparing glycine and phenylalanine mutants of conserved aromatic residues in BmK M1, we have shown that the aromatic side chains of W47F and Y35F are indispensable for maintaining the structure and pharmacological function of the toxin. Interestingly, these residues do not have to be Trp^{47} or Tyr^{35} because the aromatic side chain is the primordial component. Also indicated by this study is the fact that residue 5 has to be a tyrosine because the phenylalanine mutant displayed a very low bioactivity.

The three-dimensional structures of BmK M1 and other α-toxins reveal that Tyr^5, Tyr^{35}, and Trp^{47} are located on the three-stranded β-sheet: β_1-, β_2-, and β_3-strands, respectively. The aromatic rings of these residues are positioned orthogonally one to the other in a so-called "herringbone" arrangement (Fig. 7), which was identified as the lowest energy configuration of relatively solvent-exposed aromatic rings (26). In this way, this aromatic cluster plays an important role in the stabilization of the three-stranded β-sheet. It is plausible to infer that, due to the loss of the interactions between these aromatic rings, the β-sheet will be interrupted and maybe even disintegrated. Trp^{47} is situated at the center of the cluster (Fig. 7), and its aromatic ring resides in the vicinity of the side chains of both Tyr^5 and Tyr^{35} (distances of 3.5–4 Å). It can be hypothesized that the disruption of the herringbone arrangement due to the loss of the aromatic side chains in W47G and Y5G makes the mutants unable to express. This conclusion is supported by the fact that all of the phenylalanine mutants were very well expressed. W47F, Y35F, and Y14F also displayed the essential bioactivity (Table I). Instead of the non-expression for W47G, mutant W47F was expressed at a high level with a relative toxicity of 23%. However, the CD spectrum reveals a severe conformational change (Fig. 3*B*). In short, the glycine and phenylalanine mutants clearly indicate that, with the exception of Tyr^5, the presence of the aromatic side chain is sufficient and important for the unique structure and the pharmacological function. Tyr^5 seems to be a unique and irreplaceable amino acid. The CD spectrum shows a milder alteration for this mutant. Inspecting the three-dimensional structure, there is a contact through a hydrogen bond between the functional -OH group of Tyr^5 and the side chain of Lys^{58}/Arg^{58}, which can be found in all long chain scorpion toxins (6, 8). By consequence, an aromatic ring without that -OH group cannot maintain the general structure as shown by the CD spectrum and can interrupt the subtle tertiary arrangement between the N-terminal part and the C-terminal segment, which in turn affects the pharmacological function. Therefore, the importance of Tyr^5 is not only in the aromatic ring, but also in the functional -OH group; and as a consequence, Tyr^5 is highly conserved among α-toxins.

Aromatic Residues in Other Sites—Tyr^{14} and Tyr^{21} are located on Face B (Fig. 1*B*), which is roughly opposite to Face A, where the CHS is situated. Y14G was almost nontoxic compared with rBmK M1 (Table I). In agreement, its effect on voltage-gated sodium channels was also the least (Figs. 5 and 6). The CD spectrum was seriously altered compared with that of unmodified BmK M1 (Fig. 3*A*), indicating a conformational change due to the loss of the aromatic side chain in this position. The results show that Tyr^{14} is essential for stabilizing the unique conformation of the toxin and is involved in the interaction with the voltage-gated sodium channel. To obtain a more thorough insight in this matter, a more conservative phenylalanine substitution for Tyr^{14} was constructed. Y14F was expressed in an amount comparable to that of Y14G. However, in contrast to Y14G (no detectable toxicity and $EC_{50} > 100$ μM), Y14F possesses a high bioactivity (71% relative toxicity and $EC_{50} = 3.36 \pm 0.48$ μM) (Table I). These data reveal that it is the aromatic side chain of Tyr^{14} that mainly contributes to the proper conformation and in turn affects the pharmacological function of the toxin. This residue protrudes from the loop between the β_1-sheet and the α-helix (Fig. 7). The structure shows that its aromatic ring interacts with the side chain of Ile^6, which is also a crucial conserved residue in α-toxins. The hydrophobic interactions between these two residues on the surface may play an important role in stabilizing the unique conformation of this loop so as to influence the β-sheet and the α-helix of the toxin. The effect of mutation Y21G was milder on bioactivity, on the EC_{50} in $Na_v1.5$, and on the CD spectrum (Fig. 3*A* and Table I), indicating that the aromatic residue Tyr^{21} is putatively not a crucial determinant for the structure and pharmacological function of the toxin.

REFERENCES

1. Couraud, F., Jover, E., Dobois, J. M., and Rochat, H. (1982) *Toxicon* **20,** 9–16
2. Possani, L. D., Becerril, B., Delepierre, M., and Tytgat, J. (1999) *Eur. J. Biochem.* **264,** 287–300
3. Goudet, C., Chi, C., and Tytgat, J. (2002) *Toxicon* **40,** 1239–1258
4. Gordon, D., Martin-Eauclaire, M. F., Cestele, S., Kopeyan, C., Carlier, E., Ben Khalifa, R., Pelhate, M., and Rochat, H. (1996) *J. Biol. Chem.* **271,** 8034–8045
5. Gordon, D., Savarin, P., Gurevitz, M., and Zinn-Justin, S. (1998) *J. Toxicol. Toxin Rev.* **17,** 131–159
6. Housset, D., Habersetzer-Rochat, C., Astier, J. P., and Fontecilla-Camps, J. C. (1994) *J. Mol. Biol.* **238,** 88–103
7. Li, H. M., Wang, D.-C., Zeng, Z. H., Jin, L., and Hu, R. Q. (1996) *J. Mol. Biol.* **261,** 415–431
8. He, X. L., Li, H. M., Zeng, Z. H., Liu, X. Q., Wang, M., and Wang, D.-C. (1999) *J. Mol. Biol.* **292,** 125–135
9. Krimm, I., Gilles, N., Sautiere, P., Stankiewicz, M., Pelhate, M., Gordon, D., and Lancelin, J. M. (1999) *J. Mol. Biol.* **285,** 1749–1763
10. Tugarinov, V., Kustanovich, I., Zilberberg, N., Gurevitz, M., and Anglister, J. (1997) *Biochemistry* **36,** 2414–2424
11. Zilberberg, N., Froy, O., Loret, E., Cestele, S., Arad, D., Gordon, D., and Gurevitz, M. (1997) *J. Biol. Chem.* **272,** 14810–14816
12. Sun, Y.-M., Liu, W., Zhu, R.-H., Goudet, C., Tytgat, J., and Wang, D.-C. (2002) *J. Pept. Res.* **60,** 247–256
13. Goudet, C., Huys, I., Clynen, E., Schoofs, L., Wang, D.-C, Waelkens, E., and Tytgat, J. (2001) *FEBS Lett.* **495,** 61–65
14. Xiong, Y.-M., Ling, M. H., Wang, D.-C., and Chi, C. W. (1997) *Toxicon* **35,** 1025–1031
15. Shao, F., Xiong, Y.-M., Zhu, R.-H., Ling, M. H., Chi, C. W., and Wang, D.-C. (1999) *Protein Expression Purif.* **17,** 358–365
16. Li, H. M., Zhao, T., Jin, L., Wang, M., Zhang, Y., and Wang, D.-C. (1999) *Acta Crystallogr. Sect. D Biol. Crystallogr.* **55,** 341–344
17. Fontecilla-Camps, J. C., Habersetzer-Rochat, C., and Rochat, H. (1988) *Proc. Natl. Acad. Sci. U. S. A.* **85,** 7443–7447
18. Ito, H., Fukuda, Y., Murata, K., and Kimura, A. (1983) *J. Bacteriol.* **153,** 163–168
19. Meier, J., and Theakston, R. D. G. (1986) *Toxicon* **24,** 395–401
20. Gellens, M. E., George, A. L., Jr., Chen, L. Q., Chahine, M., Horn, R., Barchi, R. L., and Kallen, R. G. (1992) *Proc. Natl. Acad. Sci. U. S. A.* **89,** 554–558
21. Liman, E. R., Tytgat, J., and Hess, P. (1992) *Neuron* **9,** 861–871
22. Fontecilla-Camps, J. C., Alamassy, R. J., Suddath, F. L., Watt, D. D., and Bugg, C. E. (1980) *Proc. Natl. Acad. Sci. U. S. A.* **77,** 6496–6500
23. Fontecilla-Camps, J. C., Almassy, R. J., Suddath, F. L., and Bugg, C. E. (1982) *Toxicon* **20,** 1–7
24. Kharrat, R., Darbon, H., Rochat, H., and Granier, C. (1989) *Eur. J. Biochem.* **181,** 381–390
25. Zilberberg, N., Gordon, D., Pelhate, M., Adams, M. E., Norris, T., Zlotkin, E., and Gurevitz, M. (1996) *Biochemistry* **35,** 10215–10222
26. Burley, S. K., and Petsko, G. A. (1988) *Adv. Protein Chem.* **39,** 125–189
27. Koradi, R., Billeter, M., and Wüthrich, K. (1996) *J. Mol. Graphics* **14,** 51–55